Pressure stability field of Mg-perovskite under deep mantle conditions: A topological approach based on Bader's analysis coupled with catastrophe theory

Filippo Parisi[a], Luciana Sciascia[b,*], Francesco Principvalle[c], Marcello Merli[b]

[a] Dipartimento di Fisica e Chimica, Università degli Studi di Palermo, Viale delle Scienze, pad. 17, 90128 Palermo, Italy
[b] Dipartimento di Scienze della Terra e del Mare, Università degli Studi di Palermo, Via Archirafi, 22, 90123 Palermo, Italy
[c] Dipartimento di Matematica e Geoscienze, Università degli Studi di Trieste, Via Weiss, 1, 34128 Trieste, Italy

ARTICLE INFO

Keywords:
Ab initio
Catastrophe theory
Critical points
Topological analysis
Perovskite
Bader analysis
D'' region
Deep mantle
High pressure
HF/DFT

ABSTRACT

The pressure stability field of the Mg-perovskite phase was investigated by characterizing the evolution of the electron arrangement in the crystal. Ab initio calculations of the perovskite structures in the range 0–185 GPa were performed at the HF/DFT (Hartree-Fock/Density Functional Theory) exchange–correlation terms level. The electron densities, calculated throughout the ab-initio wave functions, were analysed by means of the Bader's theory, coupled with Thom's catastrophe theory. To the best of our knowledge the approach is used for the first time. The topological results show the occurrence of *two topological anomalies at P∼20 GPa and P∼110 GPa* which delineate the pressure range where Mg-perovskite is stable.

The paper accomplishes the twofold objectives of providing a contribution in shading light into the behaviour of the dominant component of the Earth's lower mantle across the D'' layer and of proposing a novel approach in predicting the stability of a compound at extreme conditions.

1. Introduction

The behaviour of minerals under high pressure conditions is attracting a growing scientific interest in earth science [1–10]. In the present work our attention is focused on Mg-perovskite ($MgSiO_3$) [11,12] due to its predominant presence in the lower mantle [13–16] and to the almost proven connection between several major seismological characteristics of the D'' region and the phase transition from $MgSiO_3$ perovskite to a higher-pressure structure called *post-perovskite* [11,17,18].

This important phase transition was experimentally discovered in 2004 [19] through a significant change in the XRD pattern of $MgSiO_3$ perovskite at high-pressure and high-temperature conditions, corresponding to the core-mantle boundary region (2550–2700-km depth, 116–125 GPa) [20], suggesting that this seismic boundary is a phase transformation origin.

The occurrence of the *post -perovskite* phase was confirmed by ab initio calculations [20–26] and its crystal structure (space group: *Cmcm*) was determined with the aid of computer simulations of atomic positions using this XRD pattern. The details of structure determination by molecular dynamics calculations were reported in [27].

The determination of the post-perovskite boundary in $MgSiO_3$ perovskite is important to shed light on the nature of the D'' region. Although the stability of the perovskite phase under high pressure conditions was the object of several investigations, this topic still represents a challenging task for both experimental and computational works. The first report on $MgSiO_3$ post-perovskite by Murakami et al. [19] found that it exists above 125 GPa and 2500 K. Following this pioneering work, the post-perovskite phase transition boundary in pure $MgSiO_3$ was experimentally determined using different pressure standards of Pt, Au, and MgO [28–30]. The accuracy of the pressure scale used to determine experimental pressure was object of debates [31,32] since the obtained results reported transition pressures differing by more than 15 GPa.

As far as computations are concerned, computations based on density functional theory (DFT) suffer from uncertainties related with the choice of the approximation used to describe the exchange–correlation energy of electrons and of the approach used to describe ionic motion.

All those aspects are summarized in a very exhaustive review by Hirose et al. [12].

An approach based on the Bader's topological analysis [33] of the

* Corresponding author.
E-mail address: luciana.sciascia@unipa.it (L. Sciascia).

electron density, coupled with Thom's catastrophe theory, could represent a helpful tool to conveniently integrate the results of experimental and computational research and to shed light into the characterization of the pressure induced phase transition. Many works using the Bader's approach can be found in literature, starting from the milestone papers by Martín Pendás et al. and by Luaña et al. [34–36] where the topological analysis of the electron density was applied to the characterization of ionic crystal structures. Bader's theory was also used by Gibbs et al. [37–39] to characterize silica polymorphs under pressure and by Prencipe and Nestola [40] to clarify the compression mechanism of beryl.

A further step towards the understanding of the mechanism of possible breakdowns of molecules and mineral structures can be realized by introducing the concepts of the Thom's catastrophe theory in the Bader's topological analysis of the electron density. Various examples of the application of this approach in the analysis of chemical reactions can be found in the review of Polo et al. [41].

As far as is concerned the characterization of mineral phases, a study of the zinc blende to rock salt transformation in BeO is reported in Contreras-García et al. [42]. Recently, the approach was successfully applied to the characterization of the Pbca enstatite to Pbcn protoenstatite phase transition [43] and of the pressure-induced phase transitions/amorphization observed in a-quartz [44].

This kind of procedure proved particularly effective in the investigation of processes occurring in the lower mantle. In this context, Parisi et al. [45] performed a thorough characterization of the pressure-induced postspinel phase transition which is believed to be responsible for the 660 km discontinuity that defines the boundary between transition zone and lower mantle.

The present paper, which is aimed at investigating the phase transition responsible to the core-mantle boundary region, represents indeed the natural prosecution of the work of Parisi et al. [45].

More in detail, the hydrostatic compression of the Mg-perovskite phase was investigated by means of first-principles calculations, in the pressure range 0–185 GPa, and the equation of state at zero temperature was constructed. Afterwards, the evolution of the electron density in the perovskite crystal structure across the pressure-induced phase transition was investigated in terms of topology of the electron density, and a topological approach based on the catastrophe theory in the framework of the Bader's theory was applied.

It is worth highlighting that, despite the large literature in this field, the approach is applied for the first time to the Mg-perovskite system.

2. Topological analysis of the electron density and catastrophe theory: theoretical background

This section consists of a brief overview of some basic concepts and definitions of the Bader's topological analysis of the electron density ρ(r) and its connections with structural stability.

The reader can refer to the Bader's milestone book [46] and to the original papers of Bader [47,48].

The topology of the electron density is described by the curvature of ρ(r) at special points called "critical points" (CPs), where the first derivatives the electron density,∇ρ (r), vanish. These CPs are defined by the values of the three eigenvalues (λ_1,λ_2,λ_3) of the Hessian matrix of ρ(r) evaluated at the CP coordinates and are represented as (ω, σ) according to their rank, ω, i.e. the number of nonzero eigenvalues, and their signature, σ, i.e. the algebraic sum of the signs of the eigenvalues. There are four types of stable CPs:

- (3, -3) or nuclear critical point, NCP, which is a maximum in ρ(r). For all atoms, but hydrogen, it can coincide with the position of a nucleus;
- (3, -1) or Bond Critical point, BCP, where ρ(r) is maximum in the plane defined by the eigenvectors associated with the negative eigenvalues and minimum along the third axis, perpendicular to this plane. This point is located between two neighbouring atoms defining a bond between them;
- (3, +1) or Ring Critical Point, RCP, where the electron density is minimum in the plane defined by the eigenvectors associated with the positive eigenvalues and maximum along the third axis, perpendicular to this plane. This point has to be found in the middle of several bonds forming a ring.
- (3, +3) or Cage Critical point, CCP, which is a minimum in ρ(r), and the charge density increases for motion in any direction away from the point.

One of the most important results of Bader's theory consists in the integration of some concepts taken from the "Catastrophe Theory" developed by Thom [47] pointing out the connection between some topological features of the electron density and the structural stability of a molecule, thus providing an efficient tool to predict the breaking of chemical bonds in some circumstances. According to Polo et al. [41] three mechanisms of catastrophes have been recognized so far for chemical reactions, indicated as *fold, cusp* and *elliptic umbilic* catastrophes. The fold mechanism, involves the coalescence of two CP's and their consequent vanishing. The cusp catastrophe involves the transformation of the critical point of a given parity (for instance a (3,-1) critical point) into two critical points of the same parity and one of the opposite parity (in this example a (3, +1) critical point). In the elliptic umbilic catastrophe the creation of a cage structure at the transition point, i.e., the appearance of a (3,+3) critical point, occurs after a BCP/RCP coalescence. A more detailed overview of the catastrophic mechanism can be found in Merli et al. [43]. Other quantities of peculiar interest theorized by the Bader's approach involve the integration over the atomic basin Ω of some functionals of the electron density. Among these operators, we recall here the so-called "radial atomic expectation" value, GR°(Ω), defined as $GR^0(\Omega) = \int_{\Omega} r_{\Omega} \bullet \nabla\rho(r) d\tau$, where r_{Ω} is the radial distance of the electron from the nucleus. This operator represents an alternative way of counting electrons over an atomic basin, taking into account the distortion effect on the gradient field due to bond.

According to Bader [49] in the case of a free atom where the vector ∇ρ(r) and the radial vector *r* are parallel and oppositely directed the integral reaches its negative maximum value -3N(Ω), where 3 N(Ω) is the basin electron population. In a bound atom, the formation of chemical bonds distorts ∇ρ(r) and leads to a smaller overlap of r and ∇ρ(r).

Another topological quantity theoretically related to this kind of surface integrals is the so-called Shannon's information entropy I(Ω), that is $I(\Omega) = \int_{\Omega} \rho' \bullet \ln(\rho') d\tau$ where $\rho' = \rho/N$ (i.e. the density normalized to one). This quantity gives an idea of how the electron density is "structured", and how the electronic wave function is delocalized and has the property of decreasing in value when a free atom becomes bound.

3. Computational details

Ab initio simulations of the perovskite structures in the range 0–185 GPa were performed by means of the CRYSTAL09 code [50] at the HF/DFT level. The structure of $MgSiO_3$ is orthorhombic (space group *Pbnm*) with an octahedrally coordinated Si atom and a Mg atom in an irregular 8-coordination. The asymmetric unit contains four atoms i.e. Mg, Si, O_1 (apical oxygen) and O_2 (planar oxygen).

Hamiltonians based on the WC1LYP [51] scheme, with a 30% of HF exchange, which proved very effective in the simulation of high pressure structures [44,52], were used. The local functions (basis sets) to construct the multielectronic wave function are linear combination of Gaussian-type functions. In particular, predefined basis sets, available in the software's online library whose corresponding acronyms are 8-511d1G [53], 88-31G* [54] and 8-411 [55] were adopted for Mg, Si and O, respectively. The same basis set expansions were already successfully employed in the ab-initio investigation of the ringwoodite,

perovskite and periclase structures in the work of Parisi et al. [45], of which, as already stated, the present work constitutes the prosecution.

SCF convergence was controlled by using a threshold of 10^{-7} a.u. The thresholds controlling the accuracy of the calculation of Coulomb and exchange integrals [56] were set to 10^{-6} for coulomb overlap tolerance, 10^{-6} for coulomb penetration tolerance, 10^{-6} for exchange overlap tolerance, 10^{-6} for exchange pseudo-overlap in the direct space, and 10^{-12} for exchange pseudo overlap in the reciprocal space [50]. The default-pruned (55,434) grid for the calculation of the integrals, having 55 radial points and a maximum number of 434 angular points, was chosen. The reciprocal space has been sampled according to a regular sublattice with a shrinking factor IS equal to 6 corresponding to 16 k-points in the sampling of the irreducible Brillouin zone [50]. Starting from the experimental structural data (i.e. cell parameters and atom coordinates) given by Sugahara et al. [57] for $MgSiO_3$ perovskite at room temperature and P = 0.0001 GPa, the ground-state relaxed structure was determined by means of the geometry optimization routine implemented in CRYSTAL09. To address the compression mechanism, calculations were performed at different unit cell volumes (corresponding to different pressures) and the energies obtained as function of the volumes were fitted by means of the 3rd order Birch-Murnhagan equation of state. The internal coordinates were optimized at each unit cell volume by using the CVOLOPT keyword which keeps the volume constant. Convergence in the geometry optimization process was tested on the root-mean-square (RMS) and the absolute value of the largest component of both the gradients and nuclear displacements. The thresholds for the maximum and the RMS forces (the maximum and the RMS atomic displacements) were set to 0.00045 and 0.00030 a.u. and those for the maximum and the RMS atomic displacements to 0.00180 and 0.00120 a.u. Geometry optimization was terminated when all four conditions were simultaneously satisfied and restarted. The FINALRUN option was used in order to restart the optimization, keeping the integrals classification based on the new geometry, until full stable optimization is achieved.

At each cell volume, the topological analysis of the calculated electron density [33] has been performed by means of the TOPOND 09 program [58].

4. Results and discussion

The pressure evolution of the electron arrangement in the perovskite crystal structure was investigated in terms of the topology of the electron density.

The compression process was simulated by performing calculations at different unit cell volumes starting from the ground state volume (V_0 = 164,95 Å^3) until the most compressed volume (V = 115,04 Å^3). For each structure, the internal coordinated (cell parameters and atomic positions) and the energy values were obtained. The E(V) data were used to construct the corresponding equations of state.

4.1. Equation of state

Fig. 1, where the normalized lattice parameters as a function of the cell volumes are depicted, indicates that, according with experimental [59–61] and computational data [62,63] the compression of the orthorhombic perovskite is anisotropic and that the b-axis is less compressible than a- or c-axis, with a-axis slightly more compressible than c.

The E(V) data have been fitted by means of 3rd order Birch-Murnhagan equation of state.

$$E(V) = E_0 - \frac{9K_0V_0}{16}\left\{\left[\left(\frac{V_0}{V}\right)^{\frac{2}{3}} - 1\right]^3 K' + \left[\left(\frac{V_0}{V}\right)^{\frac{2}{3}} - 1\right]^2\left[6 - 4\left(\frac{V_0}{V}\right)^{\frac{2}{3}}\right]\right\} \quad (1)$$

The obtained values of V_0 (volume at minimum energy), K_0 (zero-pressure bulk modulus) and K' (pressure derivative of K at P = 0) are reported in Table 1.

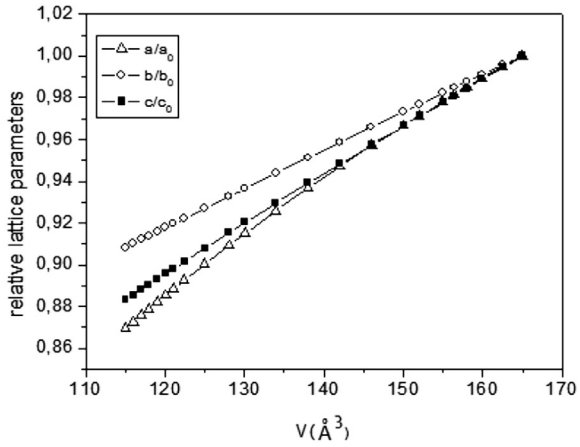

Fig. 1. Lattices parameters normalized to ground state values obtained from the optimization of the perovskite structure at the different cell volumes.

Table 1
Equation of State parameters (volume at minimum energy, V_0, zero-pressure bulk modulus K_0 and pressure derivative of K at P = 0, K') of Mg-perovskite obtained in the present study compared with previous theory and experimental studies.

V_0 (Å^3)	K_0 (GPa)	K' (10^{-3} GPa K^{-1})	References
164.9	254.5	3.9	*This study*
–	256	3.8	[64] *(experimental, 300 K)*
162.3	253	3.9	[61] *(experimental, 300 K)*
	254	4	[59] *(experimental, 300 K)*
–	266	3.9	[13] *(experimental, extrapolated at zero temperature)*
–	247	4	[65]*(experimental, 300 K)*
162.5	261	4.0	[60]*(experimental, 300 K)*
163.35	z259.82	4.06	[22] *(calculated, static, LDA)*
167.42	230.05	4.14	[22] *(calculated, static, GGA)*

The fitting parameters reported in Table 1 are in good accordance with those obtained from previous computational and experimental studies. The pressure values corresponding to each volume were determined by introducing the fitting parameters (namely V_0 and K_0) in the corresponding P(V) equations (Eq. (2)) for each volume investigated:

$$P(V) = \frac{3}{2}K_0\left[\left(\frac{V}{V_0}\right)^{-\frac{7}{3}} - \left(\frac{V}{V_0}\right)^{-\frac{5}{3}}\right]\left\{1 + \frac{3}{4}(K' - 4)\left[\left(\frac{V}{V_0}\right)^{-\frac{2}{3}} - 1\right]\right\} \quad (2)$$

In Fig. 2 the equation of state is reported, which allows to determine the correct value of pressure associated with each cell volume and therefore to identify the pressure value where critical points changes are observed.

4.2. Topological features of the atomic interactions

The Bader topological analysis applied to the electron density of the Mg-perovskite in the whole investigated pressure range revealed the presence of 11 different BCPs (5 Mg–O, 4 Si-O and 2 O–O). The complete set of BCPs is depicted in Fig. 3 where two different planes of the crystallographic cell, namely the (010) and the (001) are presented.

Some topological properties related to the BCPs, namely the electron density, ρ(r), the Laplacian of the electron density, $\nabla^2\rho(r)$, and the ellipticity ε, were investigated (Fig. 4).

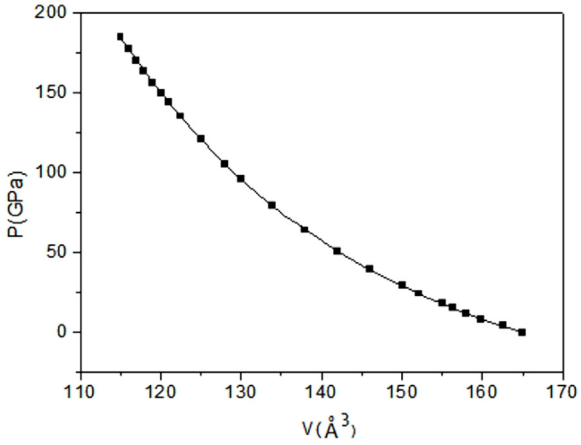

Fig. 2. Equations of states for Mg-perovskite obtained from interpolation of the 3-order Birch- Murnhagan EoS equation of state.

The trends of the topological variables as a function of the pressure are consistent with those already observed in literature [40,44,45]: as the atomic distances decrease due to the pressure load, the electron density and the Laplacian of the electron density increase as a consequence of the shortening of the bond lengths and the BCP getting closer to the nucleus.

As for the ellipticity values, it is worth to recall that, as pointed out by Bader [46], the presence of a bond with a large ellipticity in an equilibrium structure indicates the presence of an approaching instability and a change in structure. As expected, in our case, the value of the ellipticity is very large in the case of the weak O–O interactions and the lowest values are observed in the case of the stronger Si–O bonds.

Noteworthy, a rapid increase of ε for two Mg–O interaction can be observed at P ~ 25 GPa and P ~ 110 GPa going from lower to higher pressures and, although less pronounced, in Si-O interactions at P~ 25 GPa. Comparison with experimental data [19,28–30] reveals that the observed anomalies correspond to the stability pressure limit of the Mg-perovskite structure; therefore they could be taken as an indication of the occurrence of the two phase transitions.

As for the ellipticity values in the Si–O bonds, a sharper increase can be also at about P ~ 150 GPa, thus out of the stability range of Mg-perovskite phase. This could imply that this anomaly is not responsible for the perovskite to post-perovskite phase transition investigated in the present paper.

4.3. Evolution of the electron density in the perovskite crystal structure

Besides the analysis of the bond critical points, the investigation of the evolution of the topology of the electron density involving the ring and cage CPs revealed very interesting features. From this viewpoint, the P space can be splitted into three regions:

- 0 < P < 20 GPa, where there are 12 RCPs and 5 CCPs
- 20 < P < 110 GPa, where there are 13 RCPs and 6 CCPs
- P > 110 GPa, where there are 12 RCPs and 5 CCPs

More in detail, the topological results show the occurrence of two topological anomalies. The first, i.e. the appearance of a cage critical point (CCP1) coalescent with a ring critical point (RCP1), occurs at ~ 20 GPa and is a clear indication of the stabilization of the perovskite phase. The inverse process, observed at ~ 110 GPa, i.e. the vanishing of a different cage-ring couple (CCP2-RCP2), indicates the destabilization of this phase, and can be interpreted in the light of the perovskite to post-perovskite phase transition. In other words, starting from the stable topological configuration of perovskite observed in the pressure range 20–110 GPa, the structure goes towards a destabilization either on increasing or decreasing pressure. Since the two observed phase transitions involve the coalescence of two critical points, they can be interpreted in the light of the catastrophe theory as fold catastrophes.

Fig. 5 shows typical sketches of the perovskite structure corresponding to each pressure region, with just the CPs couples involved in these changes.

The most important topological results are summarized in Fig. 6 where the distances between the two critical points couples are reported:

Perusal of Fig. 6 illustrates how the Bader's topological analysis provides an effective tool for the *delineation of the stability field of the mineralogical phases.*

It could be noticed that this stability field match the experimental conditions of the lower mantle [19], if the positive Clapeyron slope (ranging from ~ 6 to ~ 13 MPa/K) obtained from both computational [21,22] and experimental [29,30] studies, is considered. More in detail, the pressure transition value here obtained, i.e., P = 110 GPa at T = 0 K, seems to be consistent with a low value of Clapeyron slope (about 6 MPa/K) which would give reason of the value of P = 125 at T = 2500 K reported in literature. Therefore, it is possible to assert that the obtained results give a contribution in the determination of the correct value of the Clapeyron slope, which still represents an unsolved task with important geophysical implications as evidenced from the quite wide range of values reported in literature.

Although it is certain that atomic vibrations influence to some extent the electron density, their effect was not taken into account in the present work. The accordance between obtained results and experimental observations seems to demonstrate that the atomic vibrations do not influence significantly the occurrence of the observed catastrophe. This behaviour could be indicative of a low-energy phase transition which does not require large atomic vibrations to occur.

4.4. Integrated atomic properties

In order to obtain a complete picture of the evolution of the electron density across the phase transition, two functionals of the electron

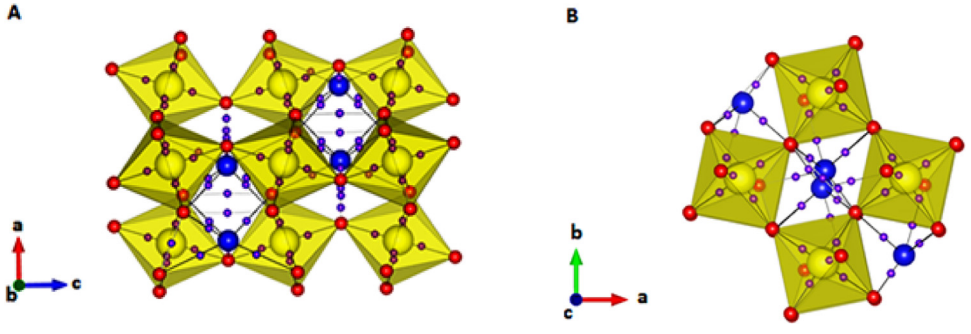

Fig. 3. Perspective projection along the (A) b-axis and (B) c-axis of the Mg-perovskite structure. *Blue spheres* Mg atoms, *yellow spheres* Si atoms, *red spheres* O atoms, violet little spheres BCPs. (For interpretation of the references to color in this figure legend, the reader is referred to the web version of this article.).

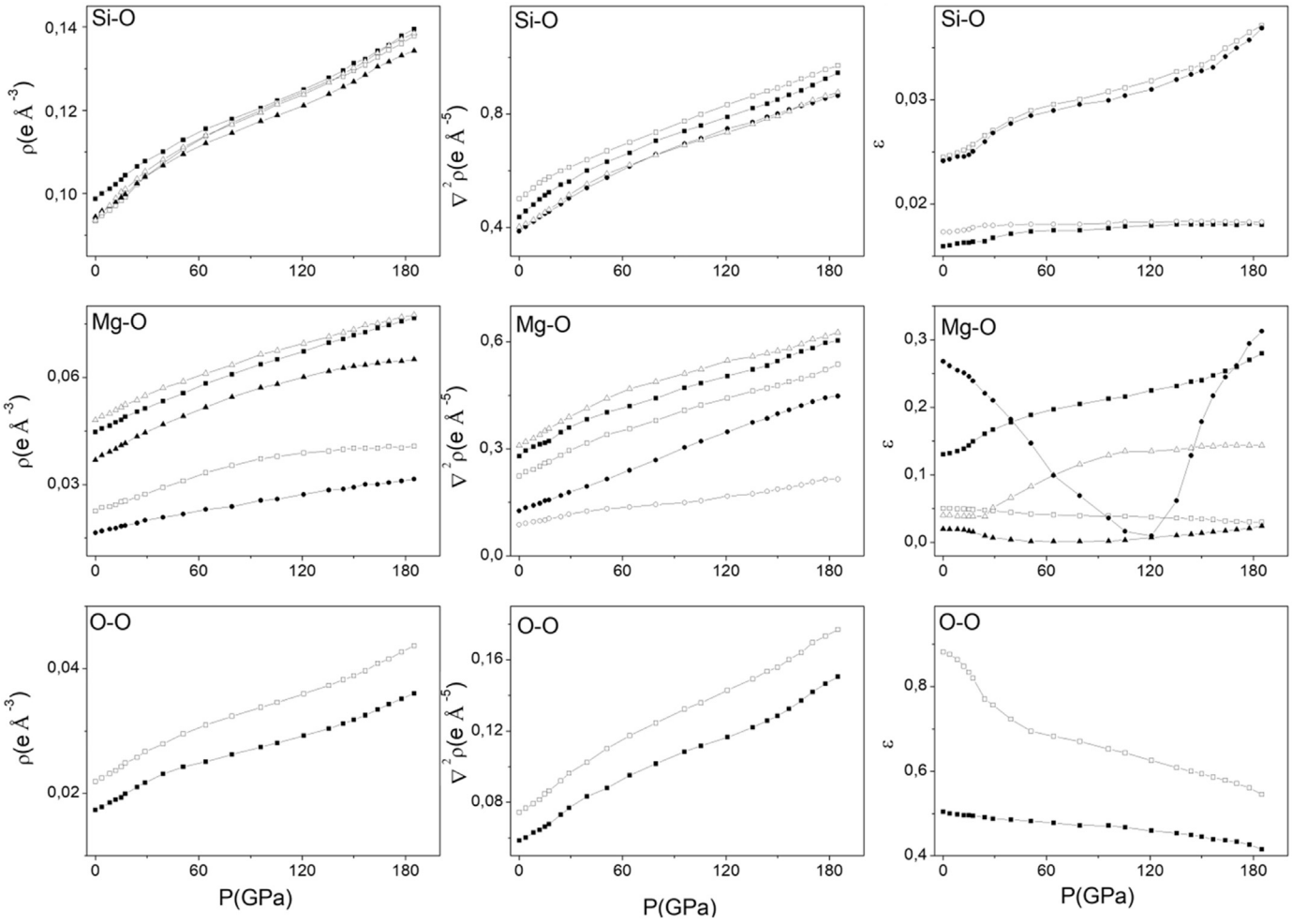

Fig. 4. Electron density, ρ, Laplacian of the electron density, $\nabla^2\rho(r)$, and ellipticity, ε, values for the BCPs related to Si–O, Mg-O and O-O interactions.

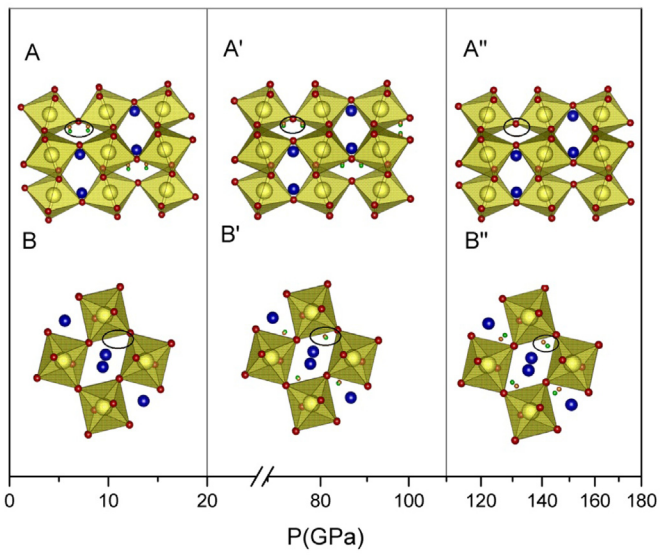

Fig. 5. Perspective projection along the (A) b-axis and (B) c-axis of the Mg-perovskite structure corresponding to each pressure region with just the CPs couples involved in these changes. CCP1-RCP1 CCP2-RCP2 couple are showed in (A) e (B), respectively. *Blue spheres* Mg atoms, *yellow spheres* Si atoms, *red spheres* O atoms, green little spheres RCPs, orange little spheres CCPs. (For interpretation of the references to color in this figure legend, the reader is referred to the web version of this article.).

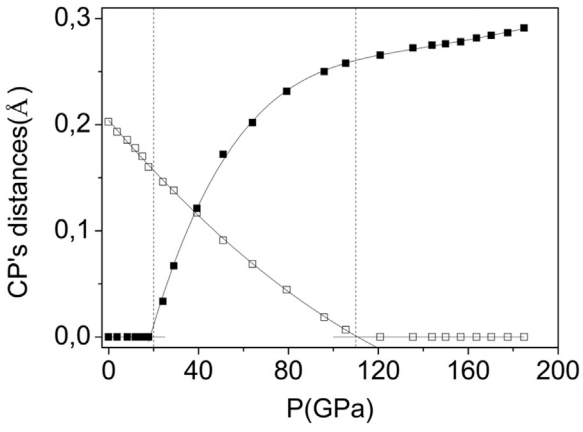

Fig. 6. Plot of the distances between the RCP1-CCP1 (empty squares) and RCP2-CCP2 (filled squares) as a function of the pressure.

density integrated over the atomic basin Ω, namely the atomic expectation value GR˚(Ω) and the Shannon entropy I(Ω), were analysed.

As already stated, the GR˚(Ω) operator measure the distortion effect on the gradient field due to bonds and it approaches the value of -3N in the case of free atom.

Looking at Fig. 7, where the ratios SPHD = GR˚(Ω) /[-3N(Ω)] for each atom are drawn, it can be seen that the operator GR˚(Ω) always integrates with a number of electrons < -3 N, which is an indication of strong interaction with neighbouring atoms.

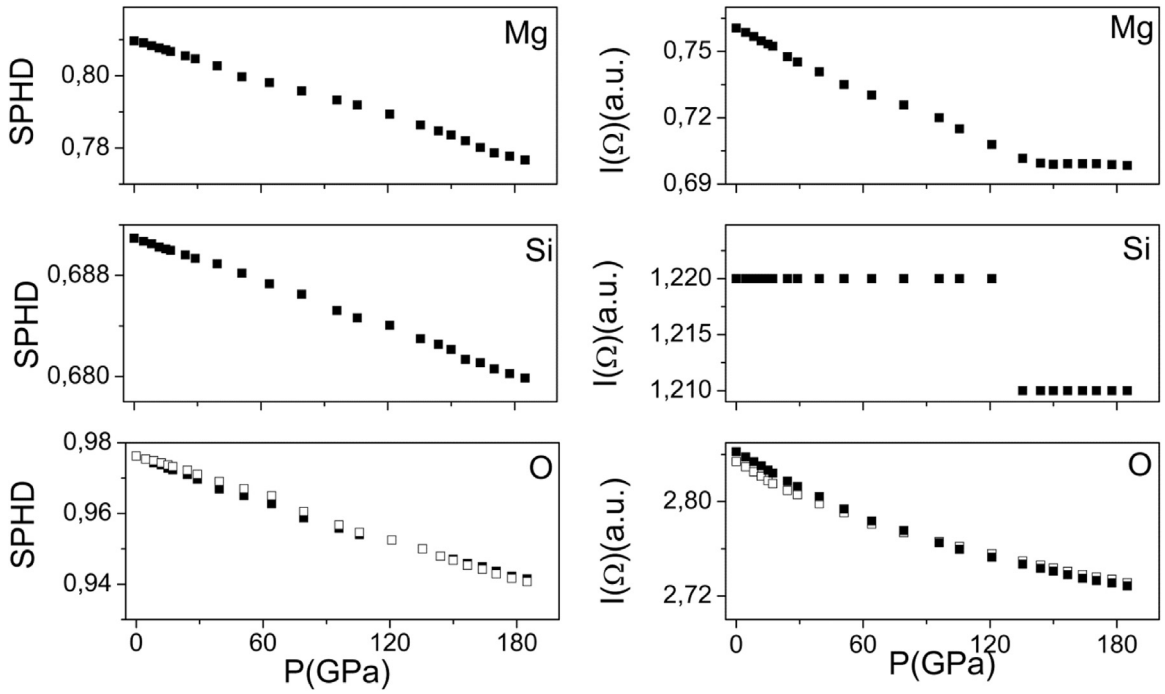

Fig. 7. SPHD ratio and Shannon entropy I(Ω) values for the atomic basins.

As expected, the difference between the value of GR˚(Ω) and -3N(Ω) is much higher for Mg and Si atom than for O.

Concerning oxygen atoms, it is interesting to highlight the difference with the behaviour previously observed by Parisi et al. [45] and Merli and Sciascia [44] where the GR˚(Ω) equals the values of -3N on approaching the pressure value corresponding with decomposition of ringwoodite structure and with amorphization of quartz structure, respectively.

The different feature observed in the present case seems to be related to the fact that the phase transition mechanism does not imply any decomposition process and could be taken as a confirmation of the occurrence of a fold catastrophe mechanism.

As for the I(Ω) operator, it has to be recalled that it provides important information about the localization of the distribution of the electronic charge density.

Perusal of Fig. 7 shows that in all the atomic basins, a decrease in the Shannon entropy values is observed due to the decrease of atomic basins volume with pressure which leads to nuclear–electron attraction increasing. While the O basin exhibits monotonically decreasing values of the missing information function, the trend for the Si and Mg basins show discontinuities at 110 GPa, which seems to record the different situations encountered across the phase transition as pressure increases, thus representing a further topological indication of the occurrence of the phase transition. It is reasonable to propose that these discontinuities are not observed in the case of oxygen atoms that have more complying electron densities than the Si and Mg atoms.

Moreover, it can be argued that the smaller value of the entropy of the electronic charge distribution for the Si atomic basin indicates a more localized charge density around this atom with respect to the Mg atomic basin. Obviously, the higher I(Ω) value for the oxygen shows that this atom has a much more delocalized electronic charge distribution due to necessity to bind, at one time, both cations and other oxygens.

5. Conclusions

An approach based of the Bader's topological analysis of the ab-initio computed electron density, coupled with Thom's catastrophe theory, was successfully applied for the first time to the characterization of the Mg-perovskite phase under high pressure conditions at 0 K.

The topological results show the occurrence of *two topological anomalies* at P ~ 20 GPa and P ~ 110 GPa which delineate the stability field of *Mg-perovskite*. The stability field observed in present work matches the experimental conditions of the lower mantle boundaries and confirms the Clapeyron slopes values observed for the post-spinel and perovskite-post perovskite phase transitions.

It is worth to underline the important geophysical implication of these results. In particular, the second observed catastrophe occurs at a pressure value that correspond at ~ 2900 km depth, exactly to the "*D"-layer*". In this region, seismic observations provide evidence of heterogeneities in wave propagation and sound velocities. In various works the perovskite to post-perovskite phase transition that occur at these pressures is invoked as the reason for these heterogeneities.

Besides providing a contribution in shading light into the behaviour of the dominant component of the Earth's lower mantle across the D" layer, the paper accomplish the important objective of proposing a powerful successful method for the investigation and the prediction of phase changes or phase breakdowns occurring under conditions at which laboratory experiments are extremely difficult, such as those of the lower mantle phases.

Acknowledgments

This research is supported by CISC—"Centro Interdipartimentale per le Scienze Computazionali dell'Università di Trieste" and by the CINECA award under the ISCRA initiative with the availability of high performance computing resources (IsC59_BTAHNS, IsC06_BTAEDPP).

References

[1] F. Nestola, T. Balić-Žunić, M. Koch-Müller, L. Secco, F. Princivalle, F. Parisi, A. Dal Negro, High-pressure crystal structure investigation of synthetic Fe_2SiO_4 spinel, Mineral. Mag. 75 (2011) 2649–2655, https://doi.org/10.1180/minmag.2011.075.5.2649.

[2] O. Adjaoud, G. Steinle-Neumann, S. Jahn, Transport properties of Mg2SiO4 liquid at high pressure: physical state of a magma ocean, Earth Planet. Sci. Lett. 312 (2011) 463–470, https://doi.org/10.1016/j.epsl.2011.10.025.

[3] O. Adjaoud, G. Steinle-Neumann, S. Jahn, Mg_2SiO_4 liquid under high pressure from

molecular dynamics, 8th Silic Melt Workshop 256 (2008) 185–192, https://doi.org/10.1016/j.chemgeo.2008.06.031.
[4] M. Koch-Müller, S.S. Matsyuk, D. Rhede, R. Wirth, N. Khisina, Hydroxyl in mantle olivine xenocrysts from the Udachnaya kimberlite pipe, Phys. Chem. Miner. 33 (2006) 276–287, https://doi.org/10.1007/s00269-006-0079-9.
[5] D. Belmonte, First principles thermodynamics of minerals at HP–HT conditions: MgO as a prototypical material, Minerals 7 (2017), https://doi.org/10.3390/min7100183.
[6] F. Nestola, B. Periotto, C. Anzolini, G. Andreozzi, A.B. Woodland, D. Lenaz, M. Alvaro, F. Princivalle, Equation of state of hercynite, $FeAl_2O_4$, and high-pressure systematics of Mg-Fe-Cr-Al spinels, Mineral. Mag. 79 (2015) 285–294, https://doi.org/10.1180/minmag.2015.079.2.07.
[7] F. Nestola, T. Boffa Ballaran, M. Koch-Müller, T. Balic-Zunic, M. Taran, L. Olsen, F. Princivalle, L. Secco, L. Lundegaard, New accurate compression data for γ-Fe_2SiO_4, Phys. Earth Planet. In. 183 (2010) 421–425, https://doi.org/10.1016/j.pepi.2010.09.007.
[8] F. Nestola, T. Balić-Zunić, M. Koch-Müller, L. Secco, F. Princivalle, F. Parisi, A. Dal Negro, High-pressure crystal structure investigation of synthetic Fe_2SiO_4 spinel, Mineral. Mag. 75 (2011) 2649–2655, https://doi.org/10.1180/minmag.2011.075.5.2649.
[9] J. Müller, S. Speziale, I. Efthimiopoulos, S. Jahn, M. Koch-Müller, Raman spectroscopy of siderite at high pressure: evidence for a sharp spin transition, Am. Mineral. 101 (2016) 2638–2644, https://doi.org/10.2138/am-2016-5708.
[10] F. Nestola, T. Boffa Ballaran, T. Balic-Zunic, F. Princivalle, L. Secco, A. Dal Negro, Comparative compressibility and structural behavior of spinel $MgAl_2O_4$ at high pressures: the independency on the degree of cation order, Am. Mineral. 92 (2007) 1838–1843, https://doi.org/10.2138/am.2007.2573.
[11] Y. Li, F. Deschamps, P.J. Tackley, Effects of the post-perovskite phase transition properties on the stability and structure of primordial reservoirs in the lower mantle of the Earth, Earth Planet. Sci. Lett. 432 (2015) 1–12, https://doi.org/10.1016/j.epsl.2015.09.040.
[12] K. Hirose, R. Wentzcovitch, D.A. Yuen, T. Lay, 2.05 - mineralogy of the deep mantle – the post-perovskite phase and its geophysical significance A2 – Schubert, Gerald, in: Proceedings of Treatise Geophys. Second Ed., Elsevier, Oxford, 2015, pp. 85–115.
[13] E. Knittle, R. Jeanloz, Synthesis and equation of state of (Mg,Fe) SiO_3 perovskite to Over 100 gigapascals, Science 235 (1987) 668, https://doi.org/10.1126/science.235.4789.668.
[14] A. Ricolleau, Y. Fei, E. Cottrell, H. Watson, L. Deng, L. Zhang, G. Fiquet, A.-L. Auzende, M. Roskosz, G. Morard, V. Prakapenka, Density profile of pyrolite under the lower mantle conditions, Geophys. Res. Lett. 36 (2009) L06302, https://doi.org/10.1029/2008GL036759.
[15] T. Irifune, T. Shinmei, C.A. McCammon, N. Miyajima, D.C. Rubie, D.J. Frost, Iron partitioning and density changes of pyrolite in earth's lower mantle, Science 327 (2010) 193–195, https://doi.org/10.1126/science.1181443.
[16] M. Murakami, Y. Ohishi, N. Hirao, K. Hirose, A perovskitic lower mantle inferred from high-pressure, high-temperature sound velocity data, Nature 485 (2012) 90–94, https://doi.org/10.1038/nature11004.
[17] K. Hirose, Postperovskite phase transition and its geophysical implications, Rev. Geophys. 44 (2006), https://doi.org/10.1029/2005RG000186.
[18] K. Hirose, T. Lay, Discovery of post-perovskite and new views on the core–mantle boundary region, Elements 4 (2008) 183–189, https://doi.org/10.2113/gselements.4.3.183.
[19] M. Murakami, K. Hirose, K. Kawamura, N. Sata, Y. Ohishi, Post-perovskite phase transition in $MgSiO_3$, Science 304 (2004) 855–858, https://doi.org/10.1126/science.1095932.
[20] M.E. Wysession, T. Lay, J. Revenaugh, Q. Williams, E.J. Garnero, R. Jeanloz, L.H. Kellogg, The D″ Discontinuity and its Implications, in: Core-Mantle Bound. Reg., American Geophysical Union, 1998, pp 273–297 ⟨http://dx.doi.org/10.1029/GD028p0273⟩.
[21] T. Tsuchiya, J. Tsuchiya, K. Umemoto, R.M. Wentzcovitch, Phase transition in MgSiO3 perovskite in the earth's lower mantle, Earth Planet. Sci. Lett. 224 (2004) 241–248, https://doi.org/10.1016/j.epsl.2004.05.017.
[22] A.R. Oganov, S. Ono, Theoretical and experimental evidence for a post-perovskite phase of $MgSiO_3$ in Earth's D″ layer, Nature 430 (2004) 445–448, https://doi.org/10.1038/nature02701.
[23] T. Iitaka, K. Hirose, K. Kawamura, M. Murakami, The elasticity of the $MgSiO_3$ post-perovskite phase in the Earth's lowermost mantle, Nature 430 (2004) 442–445, https://doi.org/10.1038/nature02702.
[24] T. Iitaka, T. Ebisuzaki, K. Hirose, K. Kawamura, Postperovskite phase transition of $MgSiO_3$, J. Phys. Conf. Ser. 29 (2006) 58–60, https://doi.org/10.1088/1742-6596/29/1/010.
[25] Z.-J. Liu, X.-W. Sun, C.-R. Zhang, J.-B. Hu, L.-C. Cai, Q.-F. Chen, High-pressure physical properties of magnesium silicate post-perovskite from ab initio calculations, Bull. Mater. Sci. 35 (2012) 665–672, https://doi.org/10.1007/s12034-012-0343-1.
[26] R.M. Wentzcovitch, Y.G. Yu, Z. Wu, Thermodynamic properties and phase relations in mantle minerals investigated by first principles quasiharmonic theory, Rev. Mineral. Geochem. 71 (2010) 59–98, https://doi.org/10.2138/rmg.2010.71.4.
[27] K. Hirose, K. Kawamura, Discovery of post-perovskite phase transition and implications for the nature of the D″ layer of the mantle, in: E. Ohtani (Ed.), Adv. High-Press, Geological Society of America, Mineral, 2007, , https://doi.org/10.1130/2007.2421(03).
[28] K. Hirose, R. Sinmyo, N. Sata, Y. Ohishi, Determination of post-perovskite phase transition boundary in $MgSiO_3$ using Au and MgO pressure standards, Geophys. Res. Lett. 33 (2006) L01310, https://doi.org/10.1029/2005GL024468.
[29] S. Ono, A.R. Oganov, In situ observations of phase transition between perovskite and CaIrO3-type phase in MgSiO3 and pyrolitic mantle composition, Earth Planet. Sci. Lett. 236 (2005) 914–932, https://doi.org/10.1016/j.epsl.2005.06.001.
[30] S. Tateno, K. Hirose, N. Sata, Y. Ohishi, Determination of post-perovskite phase transition boundary up to 4400 K and implications for thermal structure in D″ layer, Earth Planet. Sci. Lett. 277 (2009) 130–136, https://doi.org/10.1016/j.epsl.2008.10.004.
[31] Y. Fei, J. Van Orman, J. Li, W. van Westrenen, C. Sanloup, W. Minarik, K. Hirose, T. Komabayashi, M. Walter, K. Funakoshi, Experimentally determined postspinel transformation boundary in Mg2SiO4 using MgO as an internal pressure standard and its geophysical implications, J. Geophys. Res. Solid Earth. 109 (2004) B02305, https://doi.org/10.1029/2003JB002562.
[32] K. Hirose, Discovery of post-perovskite phase transition and the nature of D″ layer, in: Proceedings of Post-Perovskite Last Mantle Phase Transit., American Geophysical Union, 2007, pp. 19–35 ⟨http://dx.doi.org/10.1029/174GM04⟩.
[33] R.F.W. Bader, A quantum theory of molecular structure and its applications, Chem. Rev. 91 (1991) 893–928, https://doi.org/10.1021/cr00005a013.
[34] A. Martín Pendás, A. Costales, V. Luaña, Ions in crystals: the topology of the electron density in ionic materials. I. Fundamentals, Phys. Rev. B 55 (1997) 4275–4284.
[35] V. Luaña, A. Costales, A. Martín Pendás, Ions in crystals: the topology of the electron density in ionic materials.II. The cubic alkali halide perovskites, Phys. Rev. B 55 (1997) 4285–4297.
[36] A. Martín Pendás, A. Costales, V. Luaña, Ions in crystals: the Topology of the electron density in ionic materials. III. Geometry and ionic radii, J. Phys. Chem. B 102 (1998) 6937–6948, https://doi.org/10.1021/jp980906f.
[37] G. Gibbs, K. Rosso, D. Teter, M. Boisen, M.S. Bukowinski, Model structures and properties of the electron density distribution for low quartz at pressure: a study of the SiO bond, J. Mol. Struct. 485–486 (1999) 13–25, https://doi.org/10.1016/S0022-2860(99)00179-9.
[38] G.V. Gibbs, M.B. Boisen, K.M. Rosso, D.M. Teter, M.S.T. Bukowinski, Model structures and electron density distributions for the silica polymorph coesite at pressure: an assessment of OO Bonded Interactions, J. Phys. Chem. B 104 (2000) 10534–10542, https://doi.org/10.1021/jp002113a.
[39] G.V. Gibbs, A.E. Whitten, M.A. Spackman, M. Stimpfl, R.T. Downs, M.D. Carducci, An exploration of theoretical and experimental electron density distributions and SiO bonded interactions for the silica polymorph coesite, J. Phys. Chem. B 107 (2003) 12996–13006, https://doi.org/10.1021/jp030583+.
[40] M. Prencipe, F. Nestola, Minerals at high pressure. Mechanics of compression from quantum mechanical calculations in a case study: the beryl (Al4Be6Si12O36), Phys. Chem. Miner. 34 (2007) 37–52, https://doi.org/10.1007/s00269-006-0125-7.
[41] V. Polo, J. Andres, S. Berski, L.R. Domingo, B. Silvi, Understanding reaction mechanisms in organic chemistry from catastrophe theory applied to the electron localization function topology, J. Phys. Chem. A 112 (2008) 7128–7136, https://doi.org/10.1021/jp801429m.
[42] J. Contreras-García, A.M. Pendás, J.M. Recio, How electron localization function quantifies and pictures chemical changes in a solid: the B3 → B1 pressure induced phase transition in BeO, J. Phys. Chem. B 112 (2008) 9787–9794, https://doi.org/10.1021/jp800685u.
[43] M. Merli, F. Nestola, L. Sciascia, Bader's analysis of the electron density in the Pbca enstatite – Pbcn protoenstatite phase transition, Eur. J. Mineral. 23 (2011) 197–205, https://doi.org/10.1127/0935-1221/2011/0023-2089.
[44] M. Merli, L. Sciascia, Bader's topological analysis of the electron density in the pressure-induced phase transitions/amorphization in α-quartz from the catastrophe theory viewpoint, Phys. Chem. Miner. 40 (2013) 455–466, https://doi.org/10.1007/s00269-013-0583-7.
[45] F. Parisi, L. Sciascia, F. Princivalle, M. Merli, The pressure-induced ringwoodite to Mg-perovskite and periclase post-spinel phase transition: a Bader's topological analysis of the ab initio electron densities, Phys. Chem. Miner. 39 (2012) 103–113, https://doi.org/10.1007/s00269-011-0465-9.
[46] R.F.W. Bader, Atoms in Molecules. A Quantum Theory, Oxford University Press, Oxford, U.K., 1990.
[47] R. Thom, Stabilité structurelle et morphogénèse: essai d'une théorie générale des modèles, InterÉditions, Paris, 1977, //catalog.hathitrust.org/Record/000177545.
[48] T. Poston, I. Stewart, Catastrophe Theory and Its Applications, Dover Publications, 1978, ⟨https://books.google.it/books?id=iDs-zyuxQEMC⟩.
[49] R.F.W. Bader, Atoms in Molecules. International Series of Monographs in Chemistry, Oxford University Press, Oxford, 1994.
[50] R. Dovesi, V.R. Saunders, C. Roetti, R. Orlando, C.M. Zicovich-Wilson, F. Pascale, B. Civalleri, K. Doll, N.M. Harrison, I.J. Bush, P. D'Arco, M. Llunell, CRYSTAL09 User's Manual, University of Torino, Torino, 2009, 2009.
[51] Z. Wu, R.E. Cohen, More accurate generalized gradient approximation for solids, Phys. Rev. B 73 (2006) 235116, https://doi.org/10.1103/PhysRevB.73.235116.
[52] M. Prencipe, I. Scanavino, F. Nestola, M. Merlini, B. Civalleri, M. Bruno, R. Dovesi, High-pressure thermo-elastic properties of beryl ($Al_4Be_6Si_{12}O_{36}$) from ab initio calculations, and observations about the source of thermal expansion, Phys. Chem. Miner. 38 (2011) 223–239, https://doi.org/10.1007/s00269-010-0398-8.
[53] L. Valenzano, Y. Noël, R. Orlando, C.M. Zicovich-Wilson, M. Ferrero, R. Dovesi, Ab initio vibrational spectra and dielectric properties of carbonates: magnesite, calcite and dolomite, Theor. Chem. Acc. 117 (2007) 991–1000, https://doi.org/10.1007/s00214-006-0213-2.
[54] R. Nada, J.B. Nicholas, M.I. McCarthy, A.C. Hess, Pacific Northwest National Lab., Richland, WA (United States), Basis sets for ab initio periodic Hartree-Fock studies of zeolite/adsorbate interactions: He, Ne, and Ar in silica sodalite, Int. J. Quantum Chem. (1996) 809–820, https://doi.org/10.1002/(SICI)1097-461X(1996)60:4<809::AID-QUA3>3.0.CO;2-0.
[55] M.D. Towler, N.L. Allan, N.M. Harrison, V.R. Saunders, W.C. Mackrodt, E. Aprà, Ab

initio, Phys. Rev. B 50 (1994) 5041–5054.
[56] V.R. Saunders, R. Dovesi, C. Roetti, R. Orlando, C.M. Zicovich-Wilson, N.M. Harrison, K. Doll, B. Civalleri, L.J. Bush, P. D'Arco P, M. Llunell, CRYSTAL 2003 user's manual, University of Torino, Torino, 2003.
[57] M. Sugahara, A. Yoshiasa, Y. Komatsu, T. Yamanaka, N. Bolfan-Casanova, A. Nakatsuka, S. Sasaki, M. Tanaka, Reinvestigation of the $MgSiO_3$ perovskite structure at high pressure, Am. Mineral. 91 (2006) 533–536, https://doi.org/10.2138/am.2006.1980.
[58] C. Gatti, TOPOND98/08 – User Manual, 2008.
[59] N.L. Ross, R.M. Hazen, High-pressure crystal chemistry of MgSiO3 perovskite, Phys. Chem. Miner. 17 (1990) 228–237, https://doi.org/10.1007/BF00201454.
[60] H.K. Mao, R.J. Hemley, Y. Fei, J.F. Shu, L.C. Chen, A.P. Jephcoat, Y. Wu, W.A. Bassett, Effect of pressure, temperature, and composition on lattice parameters and density of (Fe,Mg)SiO_3-perovskites to 30 GPa, J. Geophys. Res. Solid Earth 96 (1991) 8069–8079, https://doi.org/10.1029/91JB00176.
[61] G. Fiquet, A. Dewaele, D. Andrault, M. Kunz, T.L. Bihan, Thermoelastic properties and crystal structure of MgSiO3 perovskite at lower mantle pressure and temperature conditions, Geophys. Res. Lett. 27 (2000) 21–24, https://doi.org/10.1029/1999GL008397.
[62] B. Karki, L. Stixrude, S. Clark, M. Warren, G. Ackland, J. Crain, Elastic properties of orthorhombic $MgSiO_3$ perovskite at lower mantle pressures, Am. Mineral. 82 (1997) 635–638.
[63] R.M. Wentzcovitch, B.B. Karki, S. Karato, C.R.S. Da Silva, High pressure elastic anisotropy of MgSiO3 perovskite and geophysical implications, Earth Planet. Sci. Lett. 164 (1998) 371–378, https://doi.org/10.1016/S0012-821X(98)00230-1.
[64] T. Katsura, S. Yokoshi, K. Kawabe, A. Shatskiy, M.A.G.M. Manthilake, S. Zhai, H. Fukui, H.A.C.I. Hegoda, T. Yoshino, D. Yamazaki, T. Matsuzaki, A. Yoneda, E. Ito, M. Sugita, N. Tomioka, K. Hagiya, A. Nozawa, K. Funakoshi, P-V-T relations of $MgSiO_3$ perovskite determined by in situ X-ray diffraction using a large-volume high-pressure apparatus, Geophys. Res. Lett. 36 (2009) L01305, https://doi.org/10.1029/2008GL035658.
[65] Y. Kudoh, E. Ito, H. Takeda, Effect of pressure on the crystal structure of perovskite-type MgSiO3, Phys. Chem. Miner. 14 (1987) 350–354, https://doi.org/10.1007/BF00309809.